Comprehensive 3GPP-Compatible Channel Model for FR2-2 Short-Range Communications for Various Indoor Environments

Yusuke Koda, Norichika Ohmi, Hiroaki Endo, and Hiroshi Harada
Graduate School of Informatics, Kyoto University, Yoshida-honmachi, Sakyo-ku, Kyoto, 606-8501 Japan
{koda@, endo@dco.cce., ohmi@dco.cce., hiroshi.harada@}@i.kyoto-u.ac.jp

***Abstract*—This paper proposes a comprehensive 3GPP-compatible channel model with statistical enhancement tailored for indoor short-range device-to-device (D2D) communications operating in the frequency range (FR) of 52.6–71.0 GHz termed FR2-2. Regardless of the existence of various channel models at this band for indoor communications, there will be a need for developing a channel model compatible with and understandable from the current 3GPP stochastic channel model (SCM) to facilitate the discussion in the 3GPP for developing such FR2-2 short-range D2D communication framework based on the fifth-generation (5G) new radio (NR). Indeed, such a futuristic vision can be foreseen from the fact that the 3GPP is discussing the evolution of sidelink, referred to as a D2D communication framework; however, there are no 3GPP SCM-compatible channel models applicable to FR2-2 short-range D2D communications. To fill this void, we propose the channel model coined 3GPPCompFR2-InS that allows us to generate channel impulse responses (CIR) for computer simulations, which is suitable for various indoor short-range D2D communication scenarios while retailing the similarity in terms of the implementation policy of the 3GPP SCM. 3GPPCompFR2-InS is verified based on the real-world measurements at the 60 GHz band from the viewpoint of both the validity of the channel model parameters and that of the statistical behavior of the generated CIRs.**

Keywords—millimeter wave communications, propagation measurement, 3GPP, FR2-2, short-range communication, sidelink communication

I. Introduction

As the fifth-generation (5G) mobile network grows and plays a significant role as a social infrastructure, more broadband, mission-critical, and low-latency applications will emerge to reach full automation of everything in our society, giving the potential to reach a sustainable future [1]. To reach this goal, the current centralized network architecture will fall short of supporting such autonomous systems, and instead, the mobile network will additionally include a decentralized architecture where distributed nodes locally communicate with each other in proximity [2]. Foreseeing such a future, the usage of the millimeter wave (mmWave) spectrum will contribute to fulfilling the rate and latency requirements of the automated systems by providing abundant bandwidth, which can be used for bandwidth-intensive wireless connectivity between local communication nodes.

In principle, the 5G new radio (NR) developed by the third-generation partnership project (3GPP) has a huge potential to realize such bandwidth-intensive and decentralized connectivity based on mmWaves as well as the centralized connectivity for the following two reasons: First, the 3GPP recently added the 52.6–71.0 GHz band termed frequency range (FR) 2-2 as an operating band [3], implying that the 5G NR can exploit the abundant bandwidth that lies in FR2-2. Second, the 3GPP started the study for enhancing the current device-to-device (D2D) communication framework termed sidelink to support the mmWave spectrum in Release 18. Therein, the evaluation methodology and beam management framework have been discussed [4]. These two facts allow us to envision the 3GPP supporting the aforementioned decentralized bandwidth-intensive connection between communication nodes leveraging the 5G NR.

Nonetheless, to the best of our knowledge, there are no comprehensive FR2-2 channel models for short-range D2D use cases that are compatible with and understandable from the current 3GPP stochastic channel model (SCM) [5]. Generally, channel models serve as a foundation for developing wireless communication systems [1] by generating channel impulse responses (CIRs), thereby allowing link-level and system-level computer simulations. Indeed, outside the 3GPP, many channel models for short-range D2D communications at this band have been developed. For example, the IEEE 802.15.3c and 11ad task groups that created the specification for 60 GHz wireless personal/local area network developed the channel models based on the Saleh-Velenziela model [6] and piece-wise linear model found by ray-tracing simulation [7], respectively. Moreover, from academia, many proposals for the D2D scenarios have been provided (e.g., [8, 9]). However, these frameworks are different from the 3GPP SCM, where the former directly generates CIRs whereas the 3GPP SCM first generates large-scale parameters (LSPs), which characterize the second-order statistics, and generates the CIRs consistent with the generated LSPs [10]. Owing to its difference and

[1] We refer to the term "channel model" as a framework that can generate CIRs numerically by focusing on its role of allowing the physical (PHY) layer waveform design of developing wireless communication systems. This is reasonable considering that the 5G NR-based D2D communication with FR2-2 is now developing, and the link-level PHY layer evaluation will be still required. We exclude the other large-scale models such as path loss models and shadowing models, which are generally used for system-level evaluation, not intensively used for link-level PHY layer evaluation.

implementation policy, developing 3GPP-compatible FR2-2 channel models for various short-range D2D use cases is necessary to facilitate the discussion on the FR2-2-based decentralized indoor short-range D2D communications in the 3GPP.

Motivated by this issue, this study develops a comprehensive channel model for indoor short-range D2D communications for FR2-2 band while retaining the implementation policy of the 3GPP SCM. The resultant 3GPP-compatible FR2-2 channel model termed 3GPPCompFR2-InS possesses the same parameter table as the 3GPP SCM (see. Table I) where the parameter values are filled to fit various indoor short-range D2D communications, which were extracted based on our real-world propagation measurement campaigns. Moreover, 3GPPCompFR2-InS equips a 3GPP SCM-like channel generation flow (see. Fig. 8) to provide an implementation guideline for channel generation based on the provided parameter table. Both the extracted parameter values and generated CIRs are tested to exhibit the statistical characteristics consistent with the measurement, thereby verifying 3GPPCompFR2-InS. Note that we recently proposed the 3GPP-compatible channel model for indoor short-range D2D communications for FR2-2 [11] and 95 GHz [12]; however, these channel models defined only one environment. As opposed to [11, 12], 3GPPCompFR2-InS proposed in this study is more comprehensive including more environmental definitions.

II. Measurement Champaigns for FR2-2 Short-Range Communicaiton Use Cases

A. Setup of Channel Sounding System

We developed a simple channel sounding system that measures power delay profiles (PDPs) of the omnidirectionally transmitted signal, which is scanned by receiver antenna rotations. Fig. 1 shows an overview of the channel sounding system. The receiver (RX) was equipped with a 25 dBi horn antenna rotatable in the azimuth plane whereas the transmitter (TX) was equipped with a 2 dBi omnidirectional antenna in the azimuth plane. This simple setting was considered backward from the short-range communication use case, where as opposed to long-range communication use cases, a strict beamforming in both RX and TX sides may not be required. Hence, in contrast to the double-directional measurements generally applied [13], we limited the angular scan to the RX side while using the omnidirectional antenna on the TX side. Moreover, this is sufficient to achieve our goal of developing a channel generation framework for FR2-2 short-range communications compatible with the 3GPP channel generation framework; hence, we determined to simplify the channel sounding system.

As the sounding technique to obtain the PDPs, we applied a Keysight channel sounding system [14], which is one of the time correlation-based channel soundings. As shown in Fig. 1, the signal generator generates the sounding signal a the center frequency of 3 GHz and a bandwidth of 2 GHz. This signal consists of the pseudo-random sequence, which is correlated to the same sequence known also in the RX side. Afterward, the sounding signal is up-converted to the radio frequency of 58.32 GHz and is received in the RX. The received signal is down-converted to a center frequency of 3 GHz and is sampled in the oscilloscope. At the same time, the oscilloscope calculates the PDPs based on the time-correlation-based sounding technique.

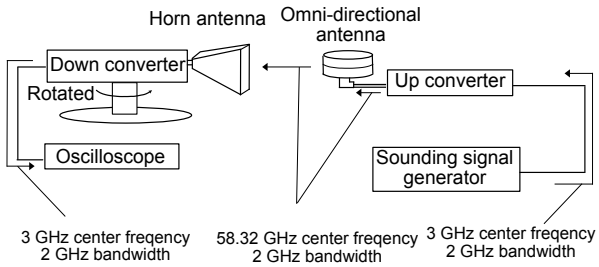

Fig. 1. Block diagram of the 60 GHz channel sounder.

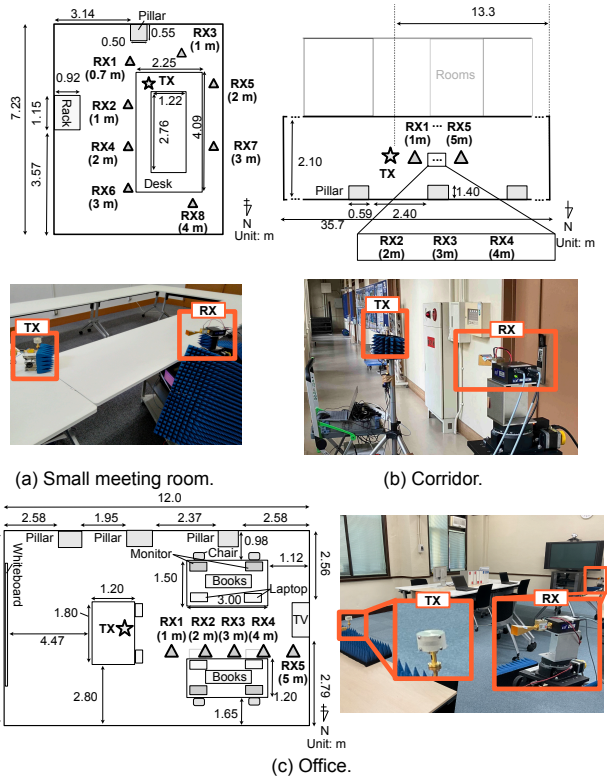

Fig. 2. Measurement environments for FR2-2 indoor short-range communication scenarios.

B. Measurement Scenarios and Environments

Small Meeting Room. This measurement was conducted in a small conference room-level indoor environment motivated by the use case of the exchange of large amounts of data between individuals in a conference room. As shown in Fig. 2(a), the room size was 5.8 m × 7.1 m. The transmitter (TX) was placed on one of the desks, which are aligned in a rectangular shape, at the height of 0.15 m. The receiver (RX) was placed at the edge of the desk with a distance of 0.7 m, 1 m, 2 m, 3 m, and 4m from the TX.

Corridor. This measurement was conducted in an indoor corridor environment, which possesses an immoderate aspect ratio compared to the aforementioned indoor rooms. Fig.

2(b) shows the overview and picture of this environment. The entire size of the corridor was 35.7 m × 2.1 m. Both TX and RX are placed at the height of 1.3 m from the ground level to consider the scenario where device-to-device communication is performed among people holding smartphones while standing on this site.

Office Room. This measurement was conducted in an office room-level indoor environment, which is larger than the small conference room-level indoor environment. It should be noted that this scenario is newly evaluated in this study in contrast to [1], which studied only the small conference room-level indoor environment. Fig. 2(c) shows the schematic overview and picture of this measurement environment. The room size was 6.8 m × 12.0 m. Inside this room, we placed office furniture, such as monitors, laptops, and books as shown in Fig. 2(c). Moreover, a whiteboard was attached to the east wall, and the television was placed on the opposite side. The TX was placed close to the center of the room, while RX was placed between the two separated office desks at a distance ranging from 1 m to 4 m from the TX.

III. Statistically-Enhanced 3GPP-Compatible Channel Model for FR2-2 Short-Range Communications

A. Model Overview

We propose 3GPPCompFR2-InS based on the model proposed for indoor short-range communication recently [11, 12]. This is performed by newly defining the model parameters that fit the FR2-2 measurement data provided in the previous section. In this section, we briefly summarize the channel model structure.

The 3GPPCompFR2-InS generates CIRs given by the following formula:

$$H(\tau,\phi)=\sum_{n=1}^{N}\sum_{m=1}^{M_n}\sqrt{P_{n,m}}\mathrm{e}^{j\Phi_{n,m}}\delta\left(t-\left(\tau_n+\tau_{n,m}\right)\right)\cdot\delta\left(\phi-\left(\phi_n+\phi_{n,m}\right)\right), \tag{1}$$

where

$$\Phi_{n,m}\sim\mathrm{uniform}(-\pi,\pi); \tag{2}$$

$$\sum_{m=1}^{M_n}P_{n,m}=P_n;\quad\sum_{n=1}^{N}P_n=1. \tag{3}$$

The indices $n\in\{1,2,\dots N\}$ and $m\in\{1,2,\dots M_n\}$ are regarding the cluster and intra-cluster subpath, respectively, where N and M_n are the number of the clusters and the number of intra-cluster subpaths in the nth cluster. N is set as the maximum observed value, and M_n is cluster-dependent value and is modeled statistically. Given these indices, τ_n, ϕ_n, P_n, $\tau_{n,m}$, $\phi_{n,m}$, and $P_{n,m}$ are the cluster excess delay in second, cluster azimuth AoA in radian, cluster sum-power, intra-cluster excess delay, intra-cluster azimuth AoA, and intra-cluster supath power, respectively, which are statistically modeled and generated. The function $\delta(\cdot)$ is the Dirac delta function. The term $\Phi_{n,m}$ is the phase term of each subpath, which are already modeled by the uniform distribution. Thus, we aim at statistically modeling the following seven components: τ_n, ϕ_n, P_n, M_n, $\tau_{n,m}$, $\phi_{n,m}$, and $P_{n,m}$, which are termed small-scale parameters (SSPs). In addition, to be compatible with the 3GPP channel model, the delay spread, angular spread, and K-factor of the generated CIRs, which are termed LSPs, are forced to be consistent with a pre-estimated statistical distribution model. These values are mathematically formulated as:

$$lgDS=\log_{10}\sqrt{\frac{\sum_{n=1}^{N}\sum_{m=1}^{M_n}\left(\tau_{n,}-\tau_{n,m}\right)^2P_{n,m}}{\sum_{n=1}^{N}\sum_{m=1}^{M_n}P_{n,m}}-\left(\frac{\sum_{n=1}^{N}\sum_{m=1}^{M_n}\left(\tau_{n,}-\tau_{n,m}\right)P_{n,m}}{\sum_{n=1}^{N}\sum_{m=1}^{M_n}P_{n,m}}\right)^2}; \tag{4}$$

$$lgASA=\log_{10}\frac{180}{\pi}\sqrt{\frac{\sum_{n=1}^{N}\sum_{m=1}^{M_n}\left(\phi_n+\phi_{n,m}\right)^2P_{n,m}}{\sum_{n=1}^{N}\sum_{m=1}^{M_n}P_{n,m}}-\left(\frac{\sum_{n=1}^{N}\sum_{m=1}^{M_n}\left(\phi_n+\phi_{n,m}\right)P_{n,m}}{\sum_{n=1}^{N}\sum_{m=1}^{M_n}P_{n,m}}\right)^2}; \tag{5}$$

$$K:=10\log_{10}\frac{P_1}{\sum_{n=1}^{N}P_n-P_1}. \tag{6}$$

Thus, the problem boils down to estimating the statistical models for LSPs and SSPs. Among these parameters, for the LSPs, cluster excess delay, cluster sum-power, and intra-cluster subpath power, we apply the same statistical model as the current 3GPP SCM [5]. Meanwhile, we proposed the amendment of the statistical models for the other SSPs [12], which is also applied to 3GPPCompFR2-InS. Due to space limitations, we only discuss the amended statistical models in the next section.

B. Amendement from 3GPP SCM

In the proposed 3GPPCompFR2-InS, we provide the amendment for the cluster azimuth AoA, the number of intra-cluster subpaths, and intra-cluster delay and intra-cluster azimuth AoA spreads in terms of their statistical models:

Cluster Azimuth AoA Distribution Model. As opposed to the fact that the original 3GPP SCM models the cluster azimuth AoA with the wrapped Gaussian model [5], in 3GPPCompFR2-InS, the cluster azimuth AoA is modeled by the uniform distribution inspired by the IEEE 802.15.3c channel model [6]:

$$\phi_n\sim\mathrm{uniform}(\phi_{\mathrm{llim}},\phi_{\mathrm{ulim}}), \tag{7}$$

where ϕ_{llim}, and ϕ_{ulim} are the lower and upper limits, respectively, which are found from the measurement data and are reported in the next section.

Model for the Number of Intra-Cluster Subpaths. As opposed to the the original 3GPP SCM modeling the number of intra-cluster subpaths as a constant value, in 3GPPCompFR2-InS, the number of subpaths are statistically modeled as the following Poisson distribution:

$$M_n-1\sim\mathrm{Poi}(\lambda_M), \tag{8}$$

where λ_M is the parameter of the Poisson distribution, which is estimated in the methodology in [12] from measurement data and is reported in the next section.

Intra-Cluster Excess Delay Model. The intra-cluster excess delay is modeled by the following uniform distribution:

$$\tau_{n,m} \sim \text{uniform}(0, 10c_{DS,n}) \quad (9)$$

where the $c_{DS,n}$ is the intra-cluster delay spread, which is further modeled as the following exponential distribution:

$$c_{DS,n} \sim \text{Exp}(\lambda_{c_{DS}}). \quad (10)$$

$\lambda_{c_{DS}}$ is the rate parameter, which is also reported in the next section. Exceptionally, when the M_n is generated to be one, $c_{DS,n}$ is forced to be zero. This is opposed to the 3GPP SCM setting $c_{DS,n}$ as a constant value.

Intra-Cluster Excess Delay Model. The intra-cluster azimuth AoA is modeled by the following uniform distribution:

$$\phi_{n,m} \sim \text{uniform}(-2c_{ASA,n,}, 2c_{ASA,n,}), \quad (11)$$

where $c_{ASA,n,}$ is the intra-cluster azimuth AoA spread and is further modeled by the following exponential distribution:

$$c_{ASA,n} \sim \text{Exp}(\lambda_{c_{ASA}}). \quad (12)$$

$\lambda_{c_{ASA}}$ is the parameter and is reported in the next section. Exceptionally, when the M_n is generated to be one, $c_{ASA,n}$ is forced to be zero. This model for $c_{ASA,n}$ is opposed to the 3GPP SCM modeling $c_{ASA,n}$ as a constant value.

C. Extracted Parameters and Statistical Validities

Table I shows the extracted statistical parameters mandatory for subsequent channel generation. Here, to extract these parameters, we applied the parameter extraction algorithm provided in [12], which is based on multipath component (MPCs) extraction, clustering, and maximum-likelihood estimation. We discuss the statistical validities for the extracted parameters as follows:

LSP Model Parameters. In 3GPPCompFR2-InS and the original 3GPP SCM, LSPs are modeled by a multivariate Gaussian distribution, and the mean, standard deviation, and correlation values are presented in Table I. Fig. 3 shows the empirical distribution of each LSP and the correlation between the arbitrary two LSPs with the estimated Gaussian distribution. The Gaussian model with the proposed parameters in Table I well captures the statistical behavior of the measured LSPs.

Delay Scaling factor r. In 3GPPCompFR2-InS and the original 3GPP SCM, the statistics of the cluster delay are modeled as an exponential distribution, and the "delay scaling factor" corresponds to its rate parameter. Fig. 4 shows the empirical distribution of cluster delay and the CDF of the exponential distribution with the estimated delay scaling factor. Note that technically, cluster delay should be scaled by the RX position-wise parameters, i.e., delay spread and constant value determined from K factor (see eq. (15) in [12]), to represent its statistics with the exponential distribution with a unique rate parameter; hence, Fig. 4(a) shows the statistics of the scaled cluster delay values. From Fig. 4(a), the exponential model with the extracted delay scaling parameter well fits the statistics of the measured cluster delay values.

TABLE I. EXTRACTED PARAMETERS FOR VARIOUS SHORT-RANGE SCENARIOS AT FR2-2.

Extracted Parameters		**Meeting room desktop**	**Corridor**	**Office**
Delay Spread DS[*1] $lgDS = \log_{10}(DS/1\text{s})$	μ_{lgDS}[*3]	-8.60	-8.58	-8.43
	σ_{lgDS}[*4]	0.34	0.24	0.26
AoA Spread ASA[*2] $lgASA = \log_{10}(ASA/1°)$	μ_{lgASA}	1.33	1.25	1.09
	σ_{lgASA}	0.28	0.17	0.34
K-Factor K [dB]	μ_{K}	11.8	6.25	12.7
	σ_{K}	6.18	5.15	7.68
Cross-correlations	ASA vs. DS	0.88	0.87	0.92
	DS vs. K	-0.94	-0.68	-0.86
	ASA vs. K	-0.95	-0.92	-0.98
Delay scaling factor r		1.29	1.89	1.20
Number of clusters N		10	13	8
Number of intra-cluster subpaths M		N/A (not represented by one value)	N/A (not represented by one value)	N/A (not represented by one value)
Parameter of Poisson distribution model for number of intra-cluster subpaths $\lambda_M^\star$		0.29	0.23	0.48
Cluster delay spread (c_{DS}) in [ns]		N/A (not represented by one value)	N/A (not represented by one value)	N/A (not represented by one value)
Parameter of exponential distribution model for cluster delay spread $\lambda_{c_{DS}}^\star$		6.05	7.88	2.83
Cluster azimuth AoA spread (c_{ASA}) in [deg]		N/A (not be represented by one value)	N/A (not be represented by one value)	N/A (not represented by one value)
Parameter of exponential distribution model for cluster azimuth AoA spread $\lambda_{c_{ASA}}^\star$		0.95	0.60	0.49
Per-cluster shadow std (ζ) in [dB]		4.84	5.47	5.01
Cluster azimuth AoA distributions		Uniform $(-5\pi/6, \pi)$	Uniform $(-13\pi/18, \pi/3)$	Uniform $(-13\pi/18, 8\pi/9)$

NOTE 1: DS denotes the root mean square (RMS) delay spread.
NOTE 2: ASA denotes the RMS azimuth spread of arrival angles.
NOTE 3: μ_{lgX} denotes the mean of the logarithmized parameter X.
NOTE 4: σ_{lgX} denotes the standard deviation of the logarithmized parameter X.

Per-Cluster Shadow Fading Standard deviation ζ. In 3GPPCompFR2-InS, the cluster power is modeled by an exponential decay model w.r.t. the cluster excess delay and the residual errors of the exponential decay line are termed per-cluster shadow fading. The per-cluster shadow fading is modeled as the zero-mean Gaussian distribution, and the standard deviation ζ is estimated from the measured data as reported in Table I. Fig. 4(b) shows the distribution of the measured per-cluster shadow fading and Gaussian distribution model with the estimated standard deviation. The model well

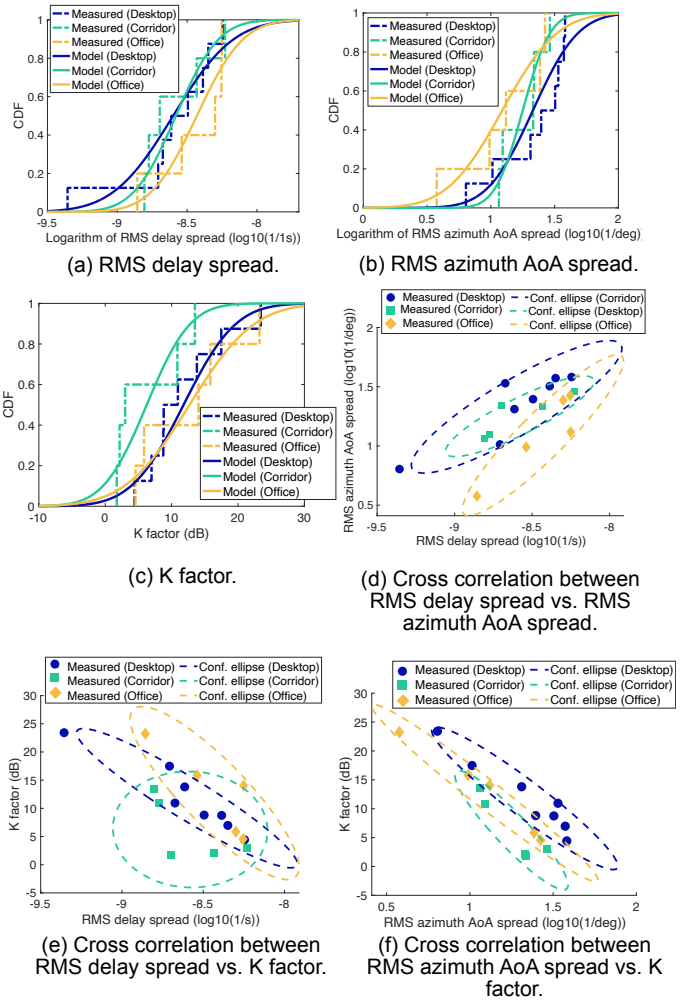

Fig. 3. Measured LSPs and multivariate Gaussian models with extracted parameters for each environment. (a)–(c) Marginal distributions of the model for each LSP and (d)–(e) Scatter plots of two LSPs with 86% confidence ellipse.

fits the measured per-cluster shadow fading, verifying the reported standard deviation parameter.

Cluster Azimuth AoA Distribution Model Parameters $\phi_{\text{llim}}, \phi_{\text{ulim}}$. The lower and upper limits of the uniform distribution model in eq. (7) is estimated from measured cluster azimuth AoAs in Table. I. As shown in Fig. 5, the uniform distribution model with the estimated upper and lower limit parameters well captures the overall statistical behavior of the cluster azimuth AoA.

Model Parameters of Number of Intra-Cluster Subpaths $\lambda_M^\star$. Fig. 6 shows the empirical distribution of the number of intra-cluster subpaths in the histogram, which were modeled by the Poisson distribution. Fig. 6 also shows the Poisson distribution with the extracted parameters in the line plot. The Poisson model with the extracted parameters fits the measured subpath distributions, verifying the extracted parameters.

Model Parameters for Intra-Cluster Delay Spread $\lambda_{c_{DS}}^\star$ and Azimuth AoA Spread $\lambda_{c_{ASA}}^\star$. Fig. 7 shows the empirical

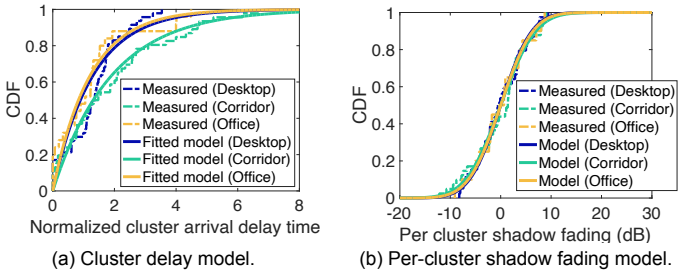

Fig. 4. Cluster delay model distributions and per-cluster shadow fading distribution models.

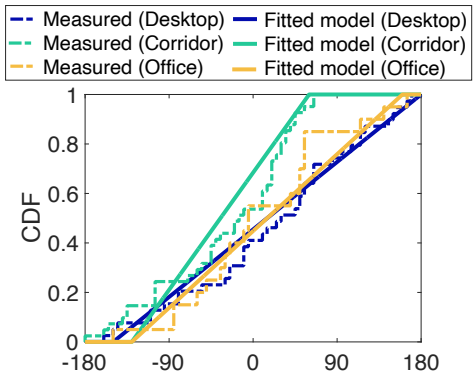

Fig. 5. Measured cluster azimuth AoA distribution and estimated uniform distribution model.

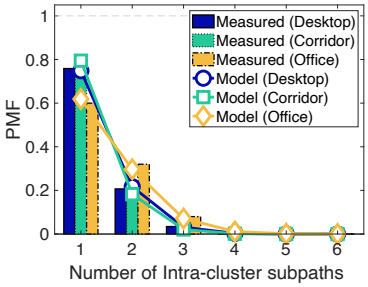

Fig. 6. Empirical distribution and statistical model of the number of observed intra-cluster subpaths.

distribution of the intra-cluster delay spread and azimuth AoA spreads, which were both modeled by the exponential distributions. Fig. 7 also shows the exponential distribution with the estimated parameters, where the statistical model captures the trend of the measured values for both intra-cluster delay and azimuth AoA spreads.

D. Overall Channel Generation Framework

Finally, in Fig. 8, we summarize the algorithmic view of the channel generation framework. First, the channel generation framework accepts the parameter table in Table I and the environment description, i.e., meeting room desktop, corridor, and office, and the parameters that match the input environment description are selected. Subsequently, the target LSPs that should be exhibited by the final channel impulse response are generated first with the multivariate Gaussian model in Fig. 8. Finally, the seven SSPs are generated according to the aforementioned statistical models with the estimated parameters in Table I for the environment of interest.

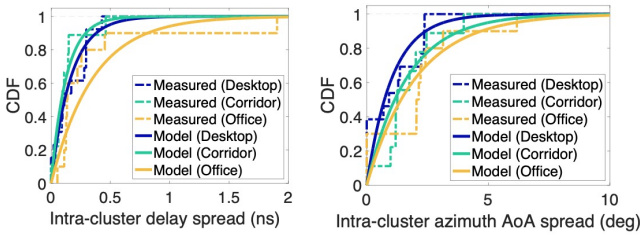

(a) Intra-cluster delay spread. (b) Intra-cluster azimuth AoA spread.

Fig. 7. Empirical distribution and estimated statistical model for the intra-cluster delay and azimuth AoA spreads.

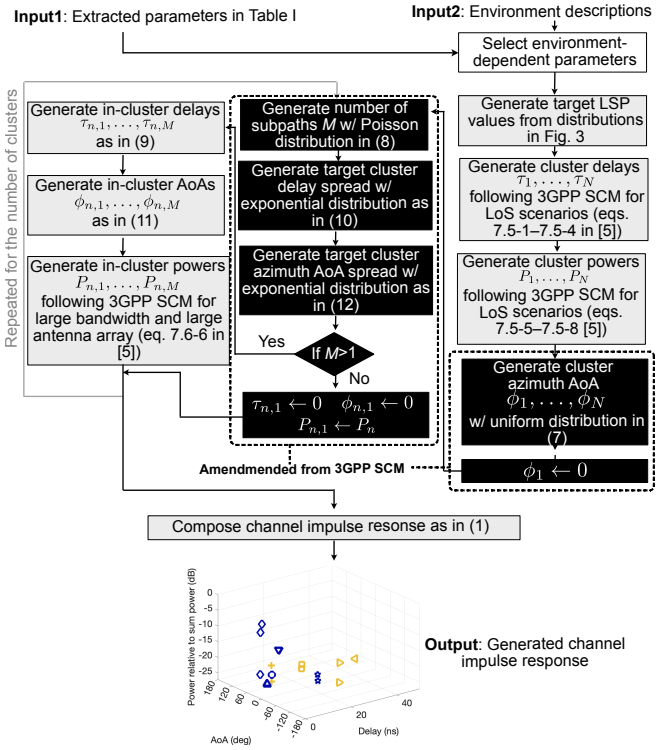

Fig. 8. Channel generation flow in 3GPPCompFR2-InS.

IV. Numerical Evaluation of Proposed Channel Model for FR2-2 Under Various Environments

This section provides the numerical evaluation of the generated channel responses with 3GPPCompFR2-InS, thereby testing the statistical consistency with the measured LSPs and intra-cluster delay and azimuth AoA spreads. This is achieved by generating the channel responses with the flow of Fig. 8 and re-calculating the LSPs and intra-cluster delay and azimuth AoA spreads from the generated channel responses. As an example, we generate 1000 channel response samples and investigate the statistical behavior of these values.

A. Statistical Validities for LSPs

Fig. 9 on the next page shows the distribution of the measured LSPs and that of the LSPs calculated by the generated channel impulse responses. These results are different from Fig. 9 in the previous section in the sense that Fig. 9 exhibits not only the validity of the parameters of Table I but also the performance of the channel generation framework whereas Fig. 3 exhibits only the statistical validity of the parameters in Table I. For all LSPs, the generated channel impulse responses exhibit the same trend of the measurement in terms of the statistical behavior of the LSPs, verifying the channel generation framework of 3GPPCompFR2-InS.

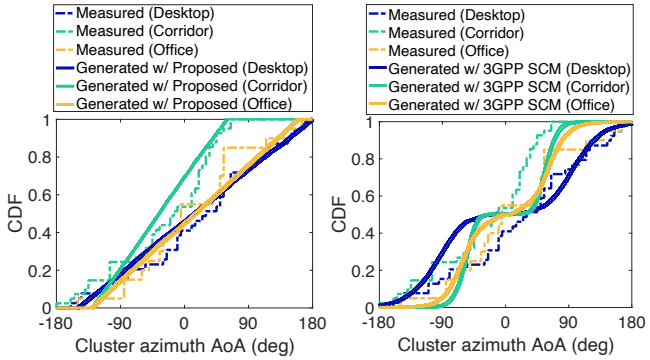

(a) Measured vs. Generated with proposed channel model. (b) Measured vs. Generated with 3GPP SCM.

Fig. 10. Cluster AoA distributions from the measurement and generated channel impulse response.

B. Statistical Validities for Amended Parameters

Finally, we investigate the benefit of the amendment provided in Section III-B by comparing it with the original 3GPP SCM [5]. As a baseline for comparison, we apply the original 3GPP SCM with the parameters in Table I and without the amendment detailed in Section III-B. Therein, the cluster AoA is modeled by the wrapped Gaussian distribution detailed in eq. 7.5-9–7.5-13 in [5] instead of the uniform distribution. Moreover, as for the number of intra-cluster subpaths M, intra-cluster delay spread c_{DS}, and intra-cluster angular spread c_{ASA}, we set these parameters to be constant values as: $M = 3$ for all environments, $c_{DS} = 0.04$ ns, 0.02 ns, 0.14 ns, and $c_{ASA} = 0.28°$, $0.32°$, $0.80°$ for meeting room desktop, corridor, and office environments, respectively, which were calculated as the average of the measured values.

Figs. 10 (a) and (b) show the distributions of the measured and generated cluster azimuth AoA values with the proposed model and 3GPP SCM, respectively. Comparing the two models, the cluster AoA distribution generated with the proposed 3GPPCompFR2-InS is shaped as a linear line owing to the uniform distribution in (7) whereas the 3GPP SCM is shaped as a multi-modal shape. From Fig. 10, we can see that the uniform distribution model does not largely deviate from the actual distribution whereas the 3GPP SCM partially exhibits a large deviation from the actual distributions. Hence, by leveraging the uniform distribution, we can generate a more similar sample to the measured cluster AoAs in terms of its statistical property.

Figs. 11 (a) and (b) show the distributions of the intra-cluster delay spreads of the channel impulse response generated by the proposed model and 3GPP SCM, respectively. Figs. 12 (a) and (b) show the distributions of the intra-cluster azimuth AoA spreads of the channel impulse response generated by the proposed model and 3GPP SCM, respectively. These figures

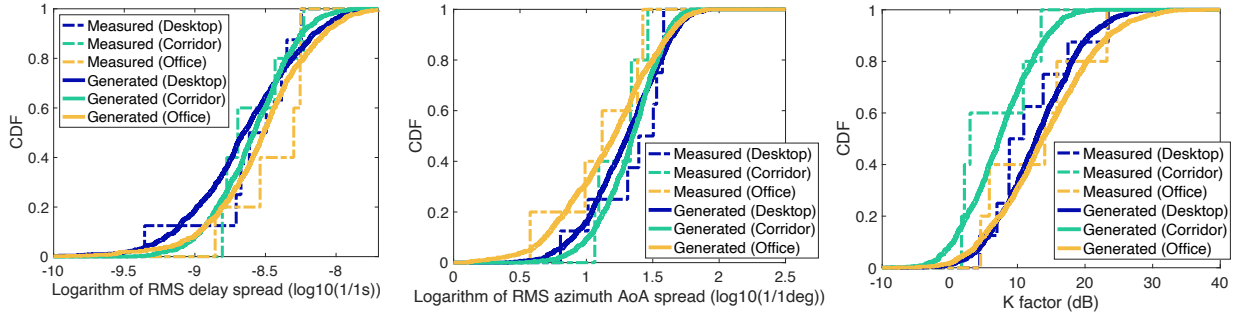

(a) RMS delay spread. (b) RMS azimuth AoA spread. (c) K factor.

Fig. 9. Measured LSPs and those calculated by the generated channel responses from the proposed model.

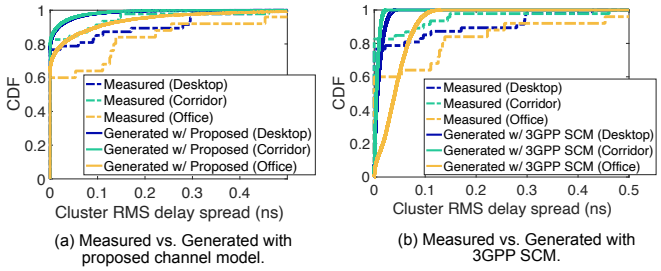

(a) Measured vs. Generated with proposed channel model. (b) Measured vs. Generated with 3GPP SCM.

Fig. 11. Intra-cluster delay spread distributions from the measurement and generated channel impulse response.

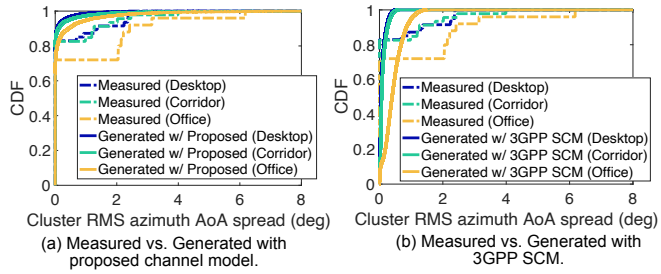

(a) Measured vs. Generated with proposed channel model. (b) Measured vs. Generated with 3GPP SCM.

Fig. 12. Intra-cluster azimuth AoA spread distributions from the measurement and generated channel impulse response.

exhibit a similar trend, where the proposed model comes close to the empirical distribution of the measured intra-cluster delay and azimuth AoA spreads in comparison with the 3GPP SCM.

V. Conclusion

This study proposed a comprehensive 3GPP-compatible stochastic channel model for indoor short-range communications operating at FR2-2 bands. To this end, we conducted the propagation measurements at the three environments for indoor short-range scenarios. Based on the measurement results, we proposed the channel model coined 3GPPCompFR2-InS that retains the 3GPP SCM structure with the amendment for the statistical models for a few parameters. Moreover, we estimated the statistically verified model parameters that fit the indoor short-range communication scenarios, which serve as the input values to generate channel impulse response accurately in the sense that the generated channel responses retain a similar statistical behavior to our conducted measurements. Numerical evaluations verified 3GPPCompFR2-InS demonstrating the generated channel impulse responses that possess the statistical properties consistent with the measurements in terms of LSPs, cluster azimuth AoAs, and intra-cluster delay and azimuth AoA spreads.

Acknowledgement

These results were obtained from the commissioned research (No. JPJ012368C04201) by the National Institute of Information and Communications Technology (NICT), Japan. A part of this research is also supported by the Ministry of Internal Affairs and Communications in Japan (SCOPE #JPJ00595).

References

[1] M. A. Uusitalo *et al.*, "6G vision, value, use cases and technologies from European 6G flagship project Hexa-X," *IEEE Access*, vol. 9, pp. 160004–160020, Nov. 2021.

[2] H. Harada, S. Mori, N. Ohmi, and Y. Koda, and K. Mizutani, "Design of 3GPP-based millimeter-wave band wireless virtual community network," in *Proc. IEEE VTC2023-Spring*, Florence, Italy, Jun. 2023, pp. 1–5.

[3] 3GPP, "NR; User equipment (UE) radio transmission and reception; Part 2: Range 2 standalone," 3GPP Tech. Specification 38.101-2, V17.7.0, Sep. 2022.

[4] 3GPP TSG RAN1 WG1, "FL summary #4 for AI 9.4.3 Enhanced sidelink operation on FR2 licensed spectrum," RAN1#114 R1-2308605, Toulouse, Flance, Aug. 2023.

[5] 3GPP "Study on channel model for frequencies from 0.5 to 100 GHz," Tech. Report 38.901, V.17.0.0, Mar. 2022.

[6] S. K. Yong, "TG3c channel modeling sub-committee final report," doc.: IEEE 15–07-0584–01-003c, Mar. 2007.

[7] A. Maltsev *et al.*, "Channel models for 60 GHz WLAN systems," doc.: IEEE 802.11-09/0334r8, May 2010.

[8] K. Haneda, J. Järveläinen, A. Karttunen, M. Kyrö, and J. Putkonen, "A statistical spatio-temporal radio channel model for large indoor environments at 60 and 70 GHz," *IEEE Trans. Antennas Propag.*, vol. 63, no. 6, pp. 2694–2704, Jun. 2015.

[9] A. Bamba, F. Mani, and R. D'Errico, "Millimeter-wave indoor channel characteristics in V and E bands," *IEEE Trans. Antennas Propag.*, vol. 66, no. 10, pp. 5409–5424, Oct. 2018.

[10] Y. Koda, R. Ouyang, N. Ohmi, and H. Harada, "Survey, taxonomy, and unification of standard mmWave channel models for WPAN, WLAN, and cellular systems in 6G," *IEEE Commun. Stan. Mag.* (accepted).

[11] Y. Koda, R. Ouyang, N. Ohmi, and H. Harada, "3GPP-compatible channel generation framework for FR2-2 indoor short-range communication," *IEEE Open J. Antennas Propag.*, vol. 4, pp. 278–293, Mar. 2023.

[12] Y. Koda, N. Ohmi, H. Endo, and H. Harada, "95 GHz indoor propagation measurement and statistically-enhanced 3GPP channel model for sub-THz indoor short-range communications," *to be submitted to Techrxiv*.

[13] M. Kim, S. Tang, and K. Kumakura, "Fast double-directional full azimuth sweep channel sounder using low-cost COTS beamforming RF transceivers," *IEEE Access*, vol. 9, pp. 80288–80299, Jun. 2021.

[14] [Online]. Available: https://www.keysight.com/jp/ja/assets/7018-05100/configuration-guides/5992-1326.pdf